

# Supporting Information

## Optimizing Platinum Location on Nickel Hydroxide Nanosheets to Accelerate Hydrogen Evolution Reaction

Qianfeng Liu,<sup>†,‡</sup> Zhao Yan,<sup>†</sup> Jianxin Gao,<sup>†,§</sup> Erdong Wang,<sup>\*,†</sup> and Gongquan Sun<sup>\*,†</sup>

<sup>†</sup>Dalian National Laboratory for Clean Energy, Dalian Institute of Chemical Physics, Chinese Academy of Sciences, Dalian 116023, China

<sup>‡</sup>University of Chinese Academy of Sciences, Beijing 100049, China

<sup>§</sup>State Key Laboratory of Fine Chemicals, School of Chemical Engineering, Dalian University of Technology, Dalian 116024, China

\*E-mail: edwang@dicp.ac.cn (E. W.).

\*E-mail: gqsun@dicp.ac.cn (G. S.).

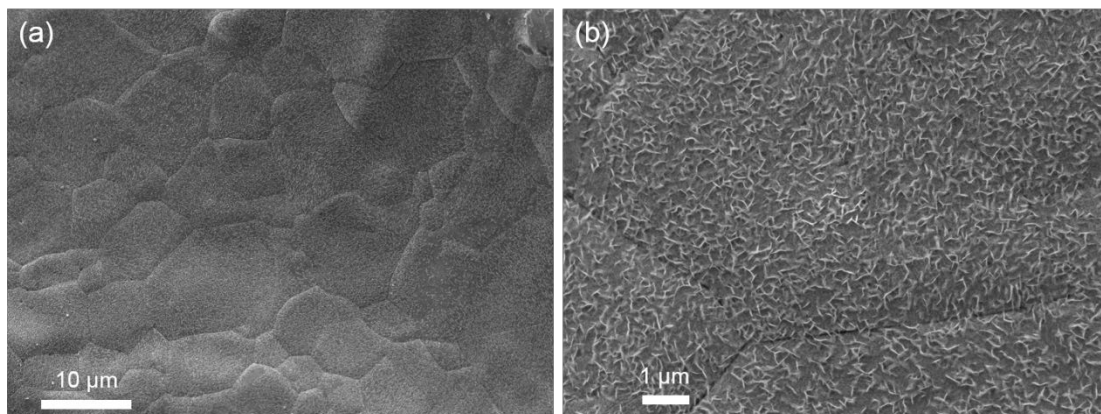


Figure S1. SEM images of Ni(OH)<sub>2</sub>-2h-NF electrode.

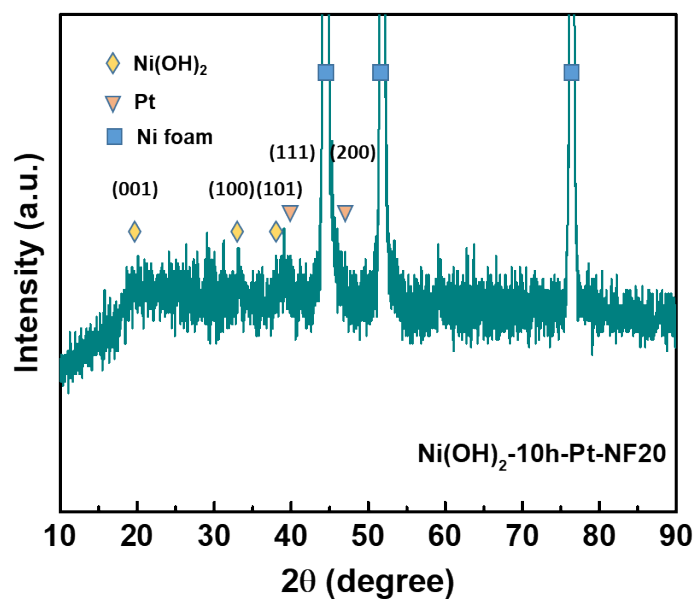


Figure S2. XRD pattern of Pt-2h-Ni(OH)<sub>2</sub>-NF20 electrode. The ultra-strong diffraction peaks presented from NF.

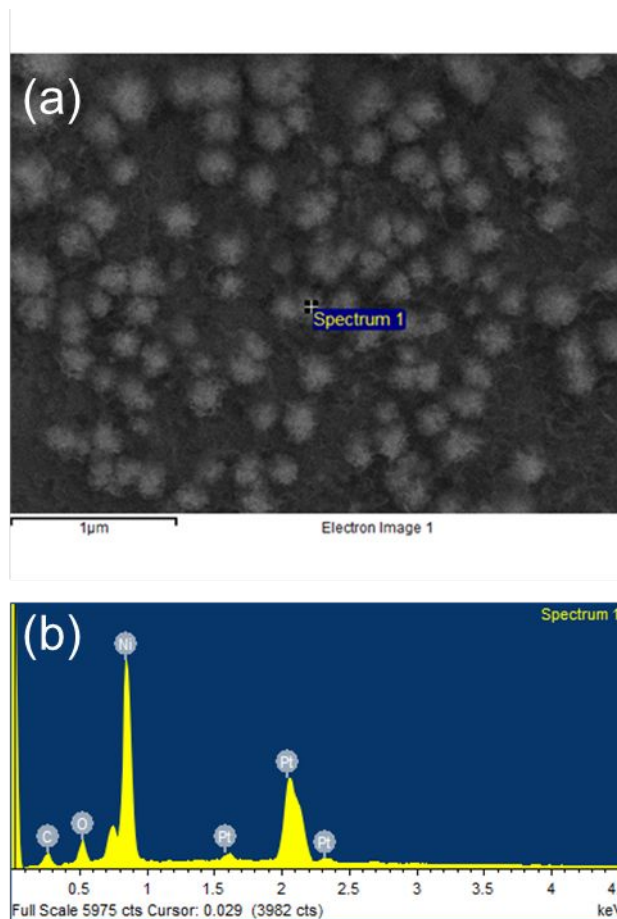


Figure S3. Determination of Pt nanoparticles. (a) SEM image of Pt-NF20 electrode and (b) the responding EDS image of the bright point.

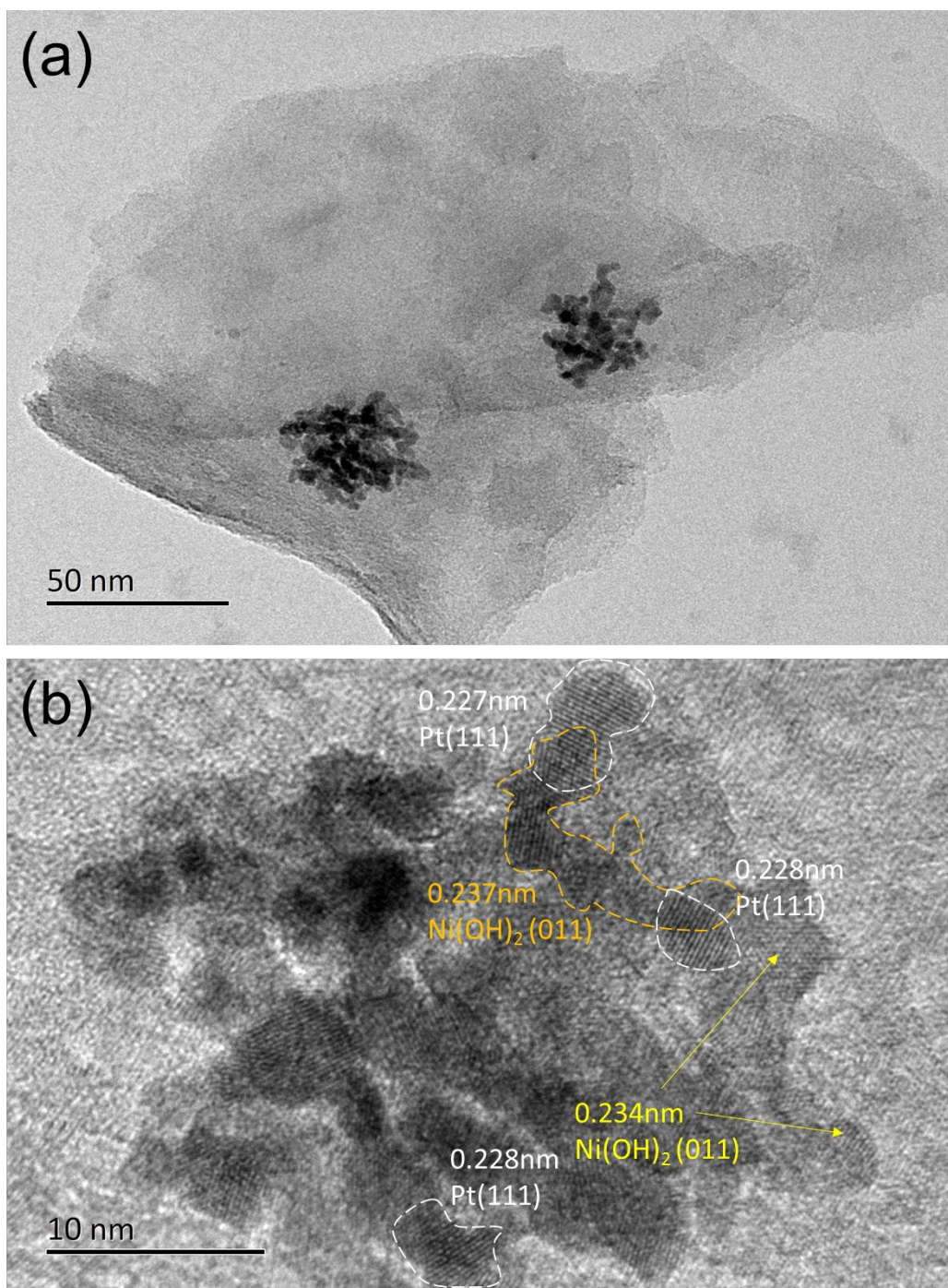


Figure S4. (a) TEM and (b) HR-TEM images of Pt-Ni(OH)<sub>2</sub>-2h-NF20 electrode.

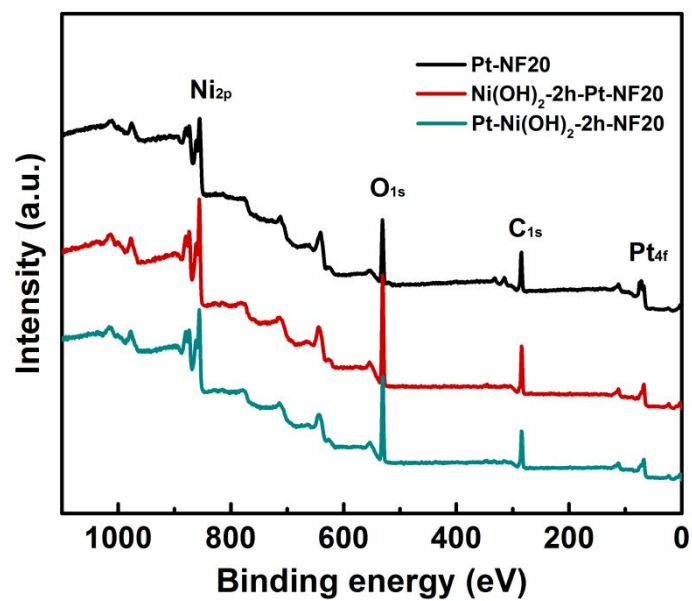


Figure S5. XPS survey spectra of Pt-NF20, Ni(OH)<sub>2</sub>-2h-Pt-NF20 and Pt-Ni(OH)<sub>2</sub>-2h-NF20 electrodes.

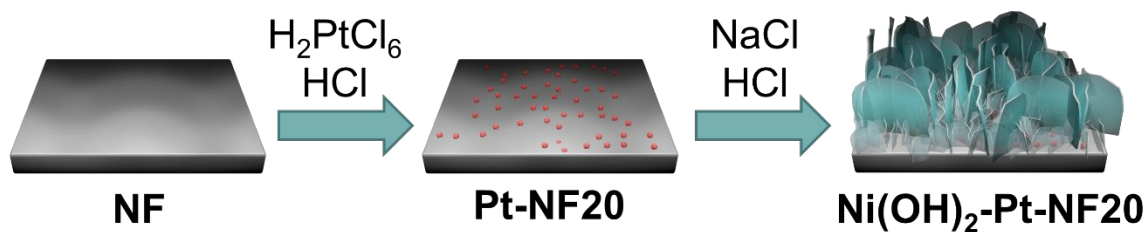


Figure S6. Schematic illustration of the synthesis for Pt-NF20 and Ni(OH)<sub>2</sub>-2h-Pt-NF20 electrodes.

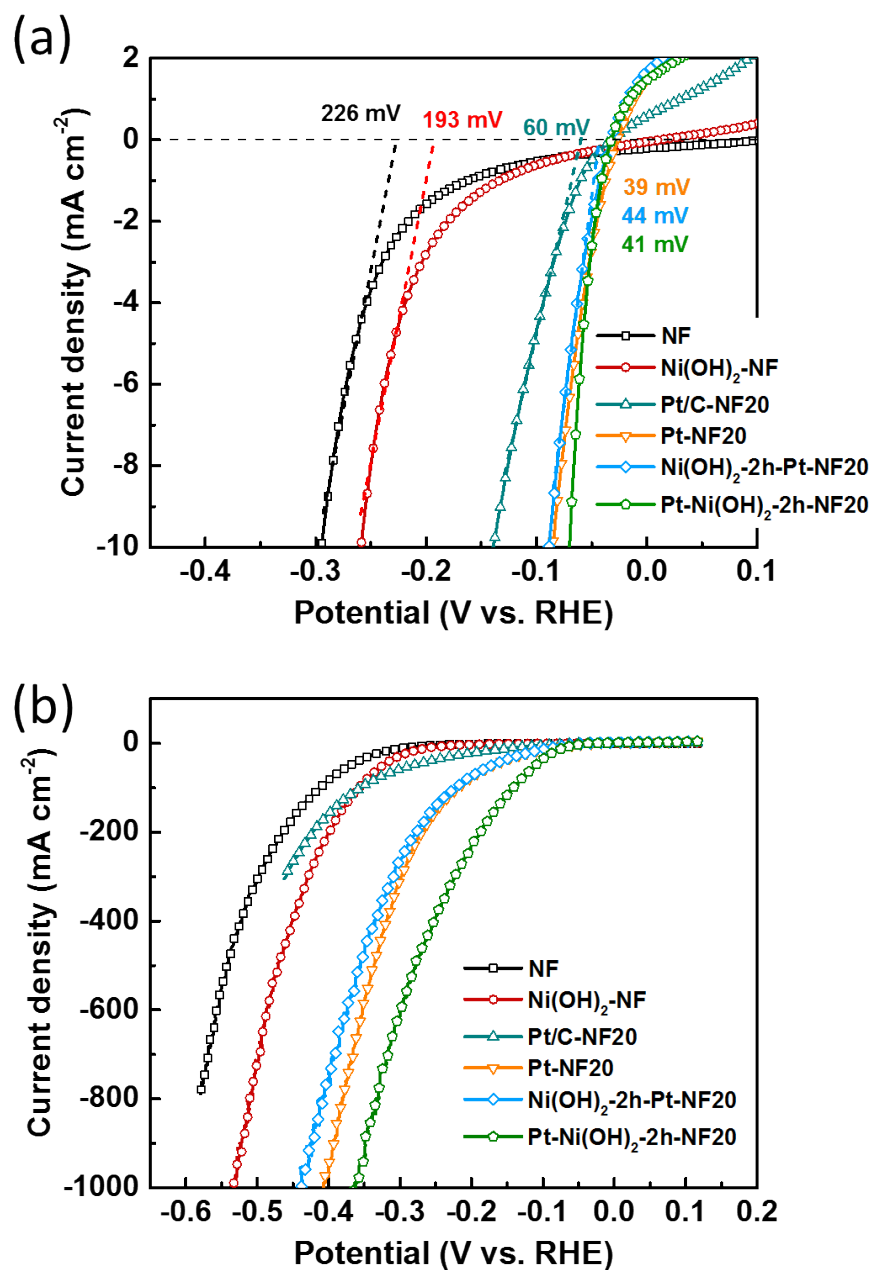


Figure S7. (a) Polarization curves and onset HER overpotentials (b) polarization curves of NF, Ni(OH)<sub>2</sub>-NF, Pt/C-NF20, Pt-NF20, Ni(OH)<sub>2</sub>-2h-Pt-NF20 and Pt-Ni(OH)<sub>2</sub>-2h-NF20 electrodes.

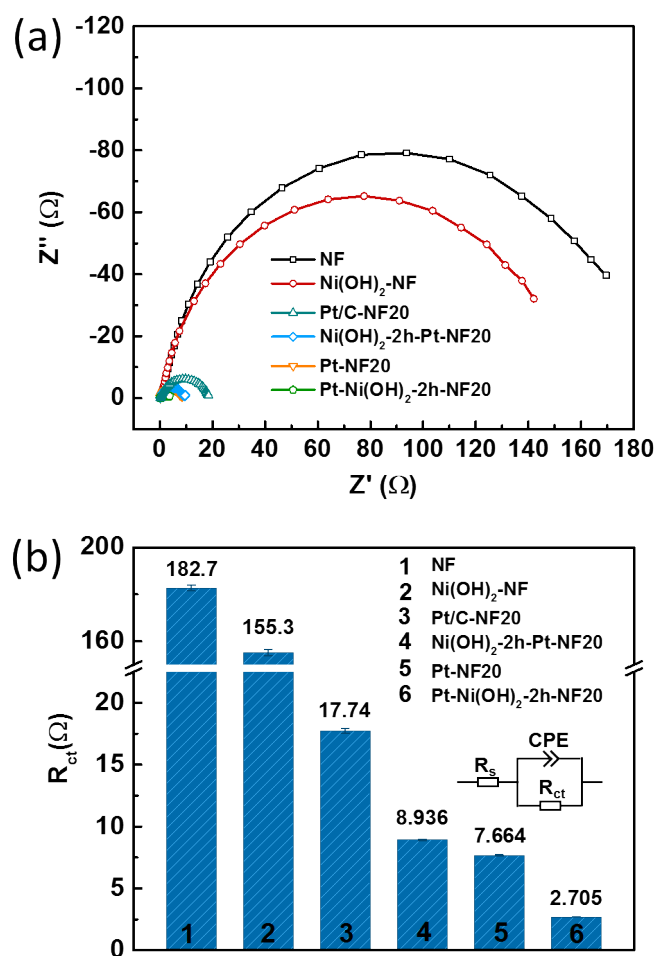


Figure S8. (a) EIS at HER overpotential of 60 mV for the NF,  $Ni(OH)_2$ -NF, Pt/C-NF20, Pt-NF20,  $Ni(OH)_2$ -2h-Pt-NF20 and Pt- $Ni(OH)_2$ -2h-NF20 electrodes. (b) Plot of charge transport resistance ( $R_{ct}$ ) of the corresponding electrodes.

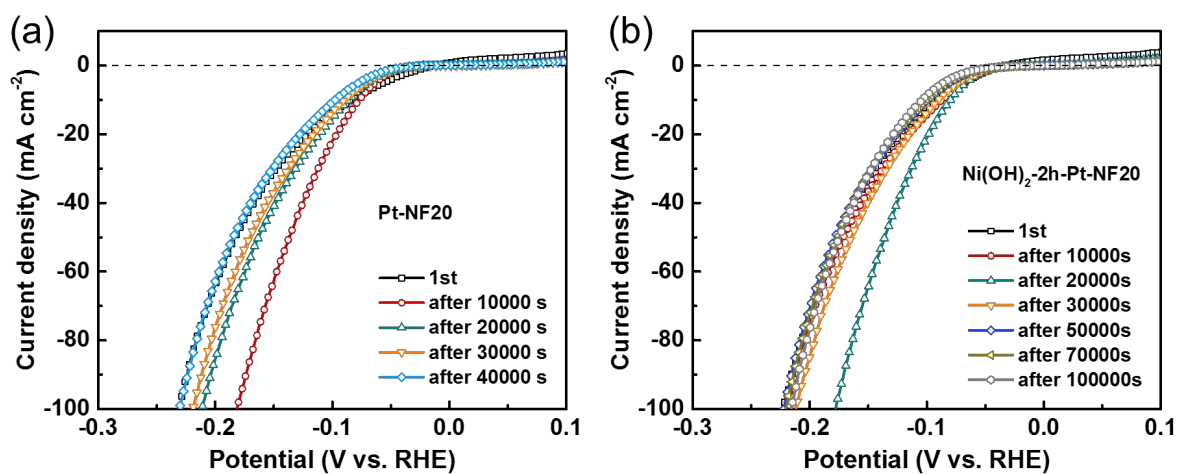


Figure S9. HER polarization curves of stability tests for (a) Pt-NF20 and (b) Ni(OH)<sub>2</sub>-2h-Pt-NF20 electrodes.

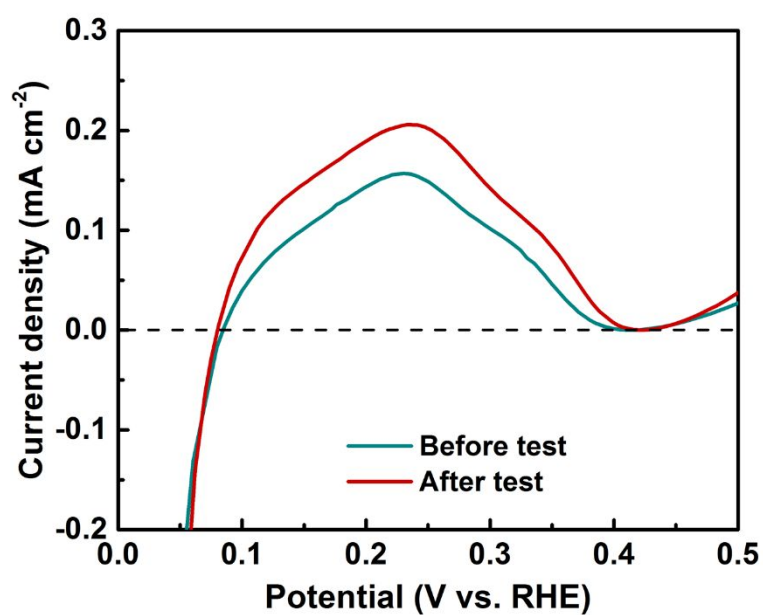


Figure S10. Partial CV curves with background correction of Pt-Ni(OH)<sub>2</sub>-2h-NF20 electrodes for ECSA of Pt in 0.1 M KOH at a scan rate of 50 mV s<sup>-1</sup> before and after stability test.

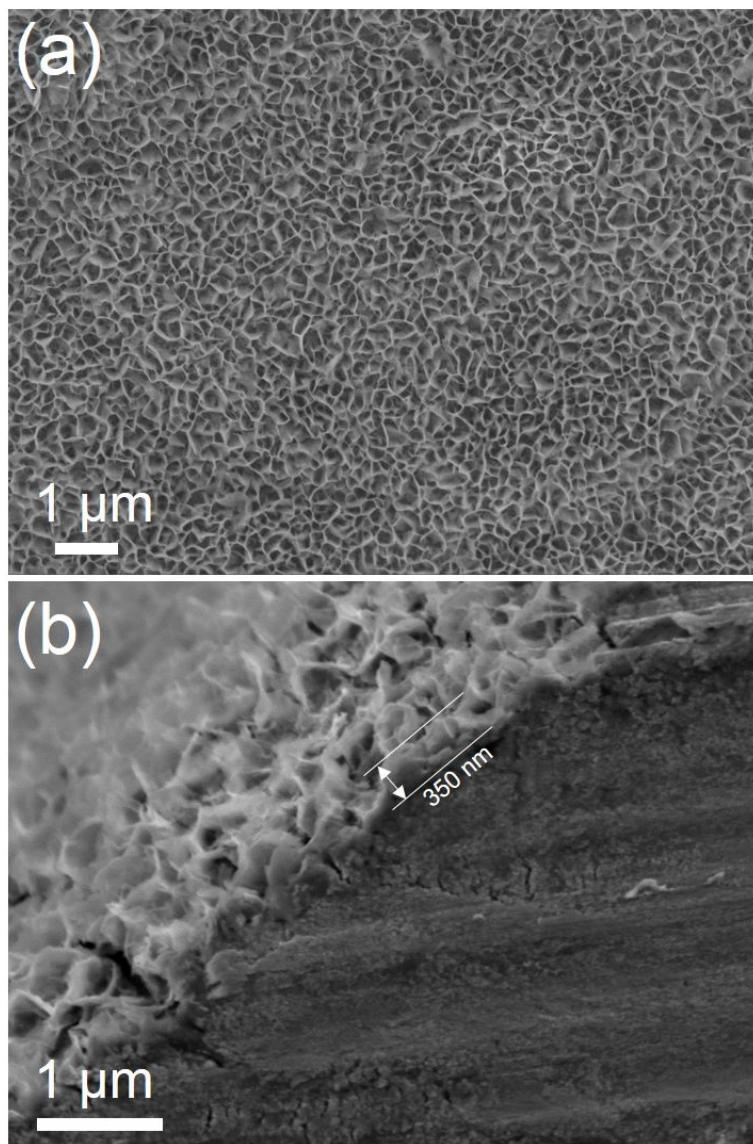


Figure S11. SEM images of Pt-Ni(OH)<sub>2</sub>-2h-NF20 electrode after 150000 s stability test.

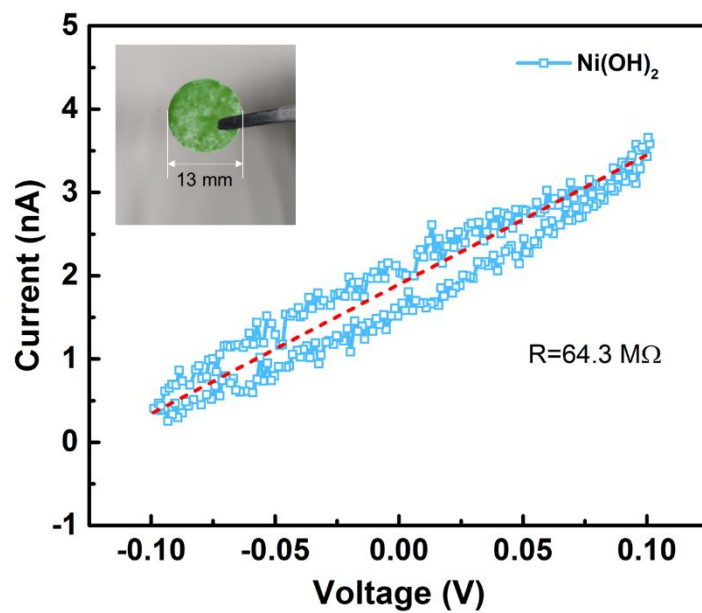


Figure S12. CV curve for testing the conductivity of  $\text{Ni(OH)}_2$  obtained from  $\text{Ni(OH)}_2$ -NF electrodes by ultrasonic treatment. Inset: photograph of  $\text{Ni(OH)}_2$  sheet with diameter of 13 mm and thickness of 0.060 mm fabricated by squash technique. The conductivity of the  $\text{Ni(OH)}_2$  sheet is  $7.07 \times 10^{-4} \text{ mS cm}^{-1}$ .

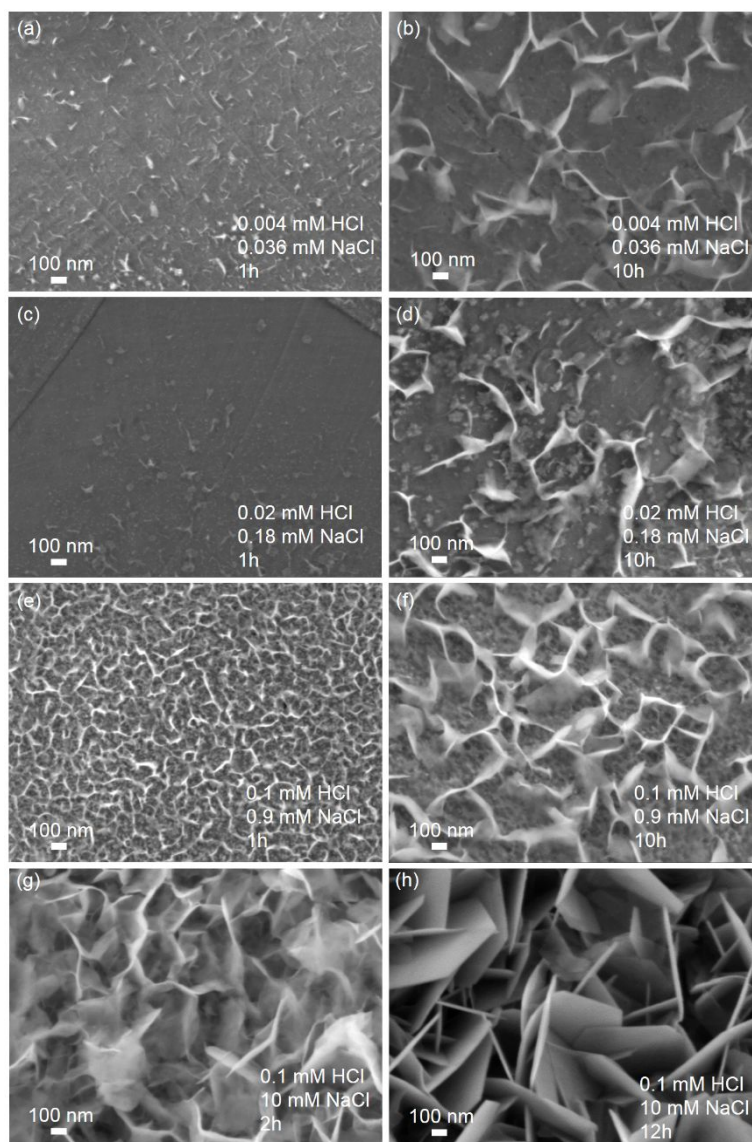


Figure S13. The optimization of concentration for HCl and NaCl to control the height of Ni(OH)<sub>2</sub> layer. The SEM images of Ni(OH)<sub>2</sub> sheets with different concentrations of HCl (0.004-0.1 mM) and NaCl (0.036-10 mM) under 40 °C with different time, the details of which were described in the images from (a) to (h).

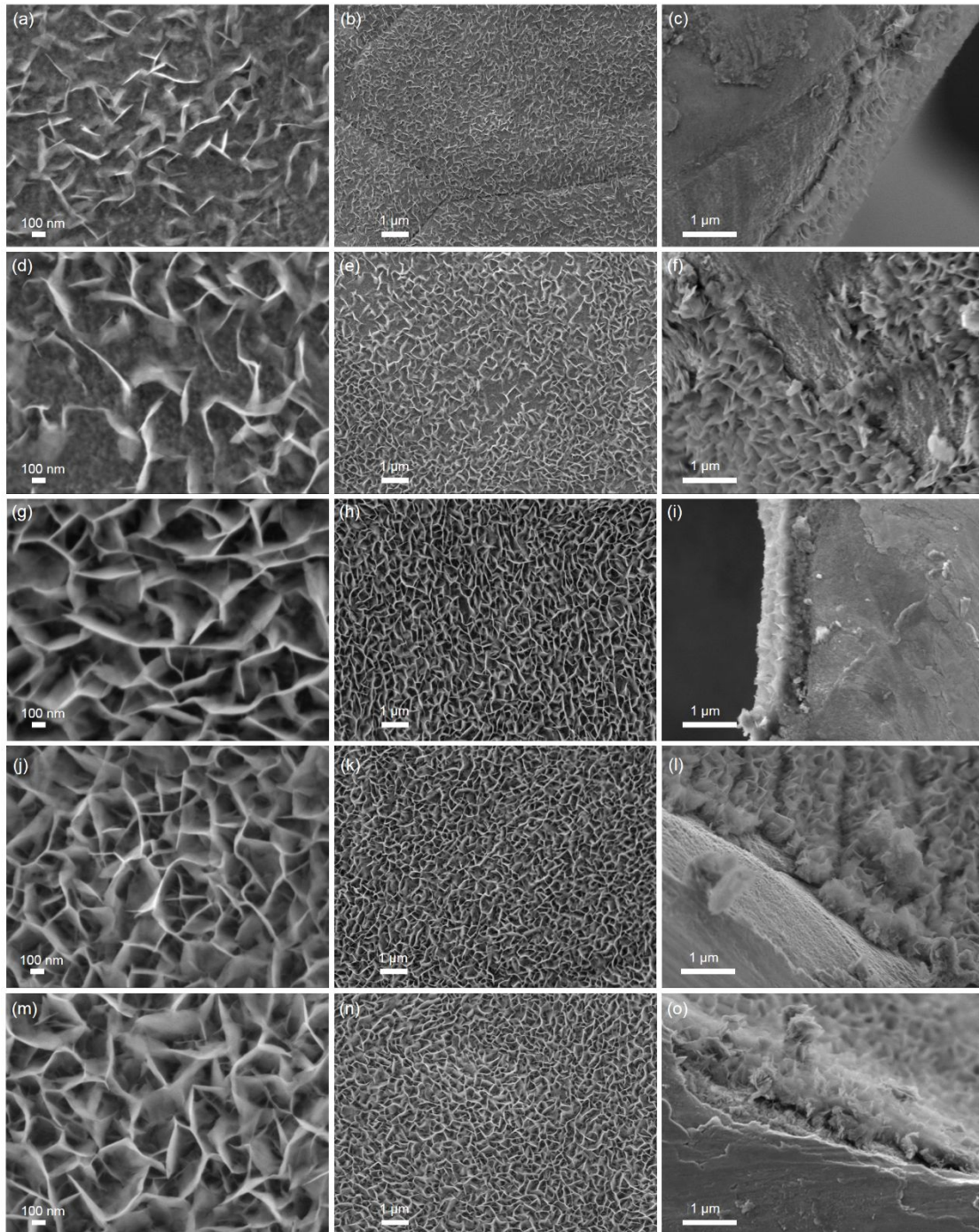


Figure S14. SEM images of (a, b, c)  $\text{Ni(OH)}_2$ -2h-NF, (d, e, f)  $\text{Ni(OH)}_2$ -4h-NF, (g, h, i)  $\text{Ni(OH)}_2$ -8h-NF, (j, k, l)  $\text{Ni(OH)}_2$ -16h-NF and (m, n, o)  $\text{Ni(OH)}_2$ -24h-NF electrodes.

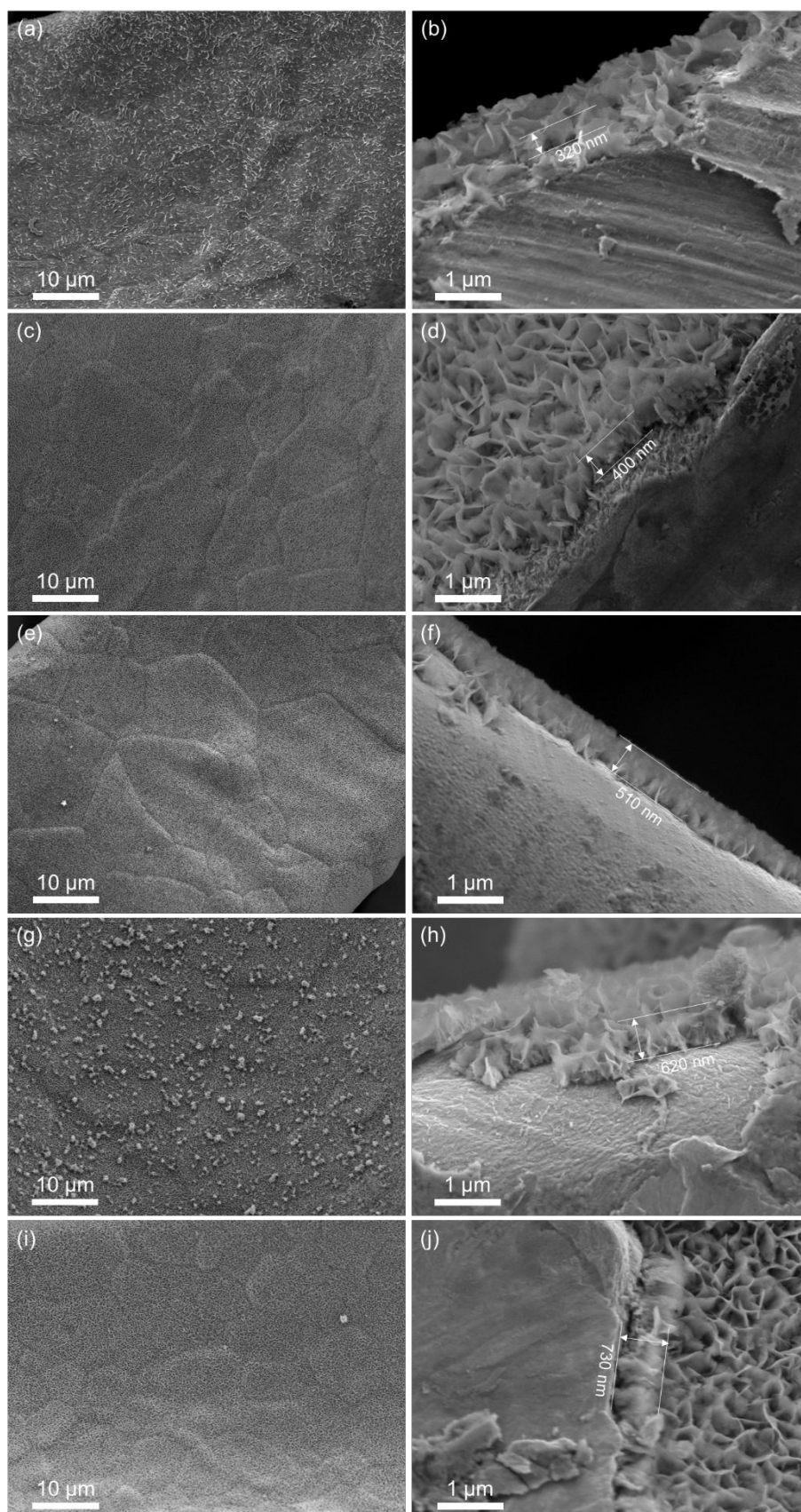


Figure S15. SEM images of (a, b) Pt-Ni(OH)<sub>2</sub>-2h-NF20, (c, d) Pt-Ni(OH)<sub>2</sub>-4h-NF20, (e, f) Pt-Ni(OH)<sub>2</sub>-8h-NF20, (g, h) Pt-Ni(OH)<sub>2</sub>-16h-NF20, (i, j) Pt-Ni(OH)<sub>2</sub>-24h-NF20 electrodes.

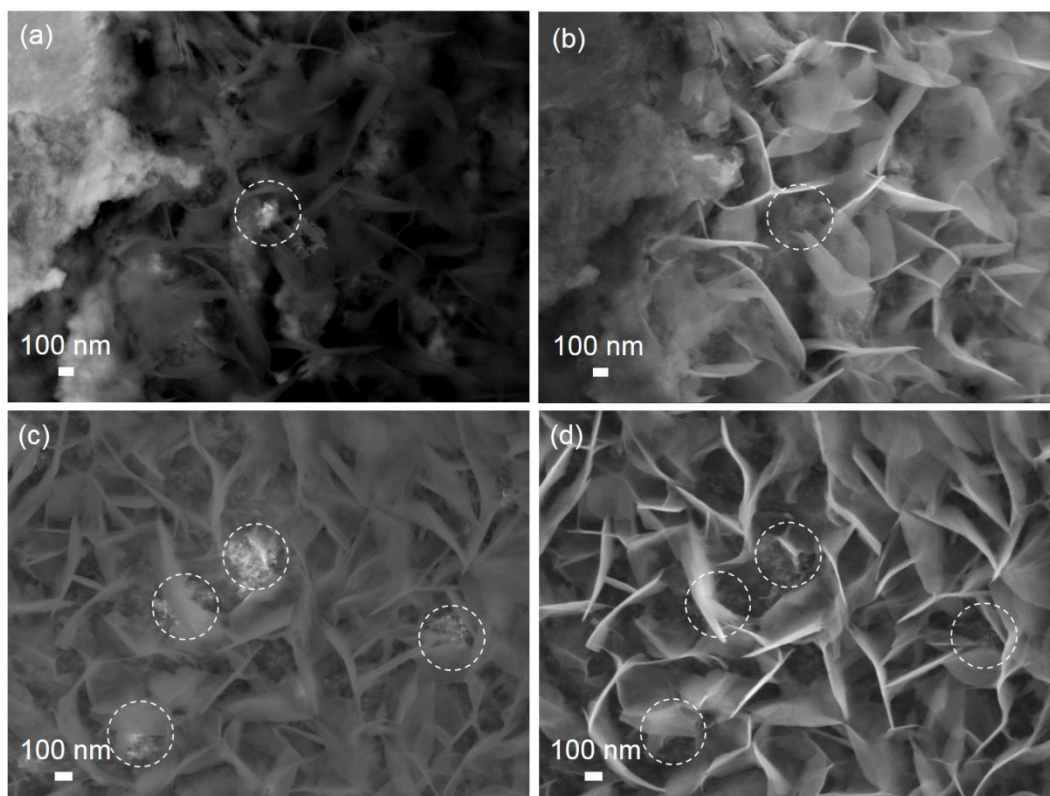


Figure S16. (a, c) SEM images of Pt-Ni(OH)<sub>2</sub>-10h-NF20 electrode on two positions and (b, d) the corresponding images under BED model to determine the location of Pt particles on the Ni(OH)<sub>2</sub> nanosheets. In the images, the dotted white circles are the positions of Pt particles.

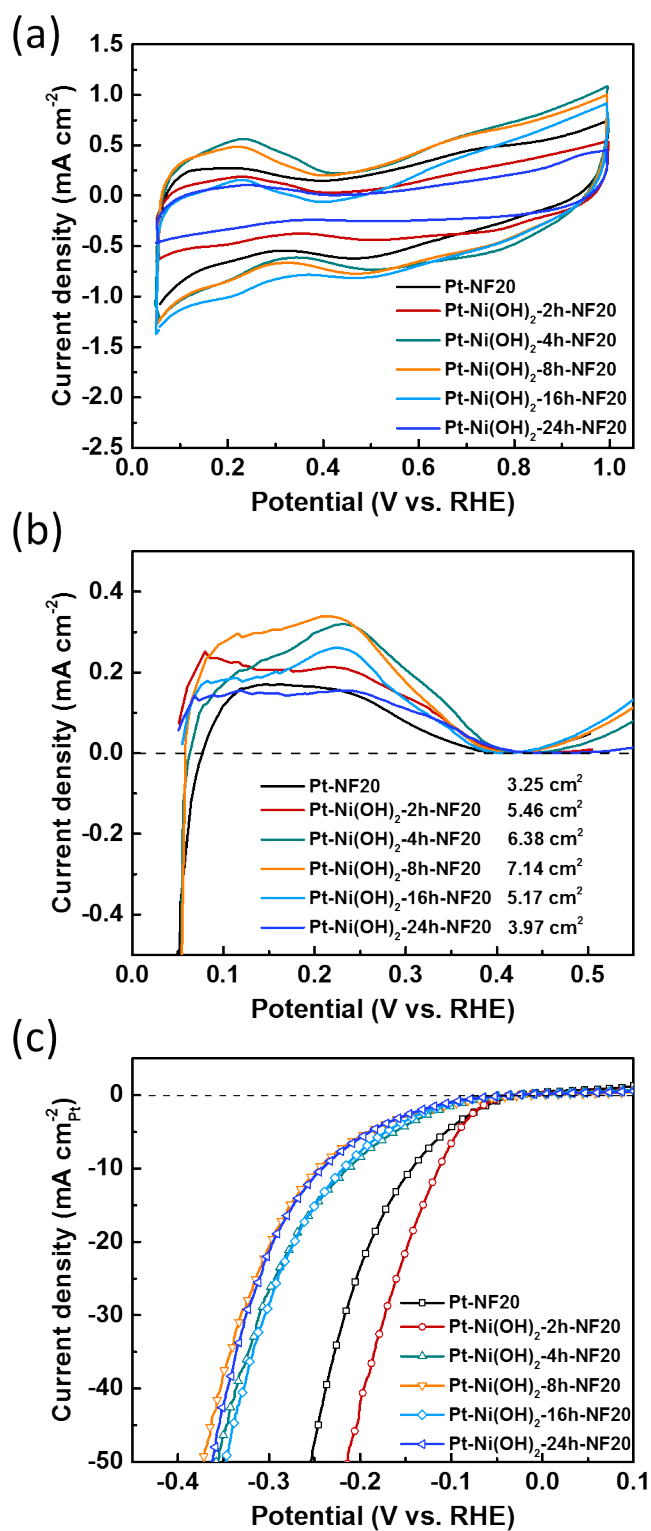


Figure S17. (a) CV curves and (b) partial CV curves with background correction of Pt-NF20, Pt-Ni(OH)<sub>2</sub>-2h-NF20, Pt-Ni(OH)<sub>2</sub>-4h-NF20, Pt-Ni(OH)<sub>2</sub>-8h-NF20, Pt-Ni(OH)<sub>2</sub>-16h-NF20 and Pt-Ni(OH)<sub>2</sub>-24h-NF20 electrodes for ECSA of Pt in 0.1 M KOH at a scan rate of 50 mV s<sup>-1</sup>. (c) The HER polarization curves normalized to ECSA of Pt for the electrodes.

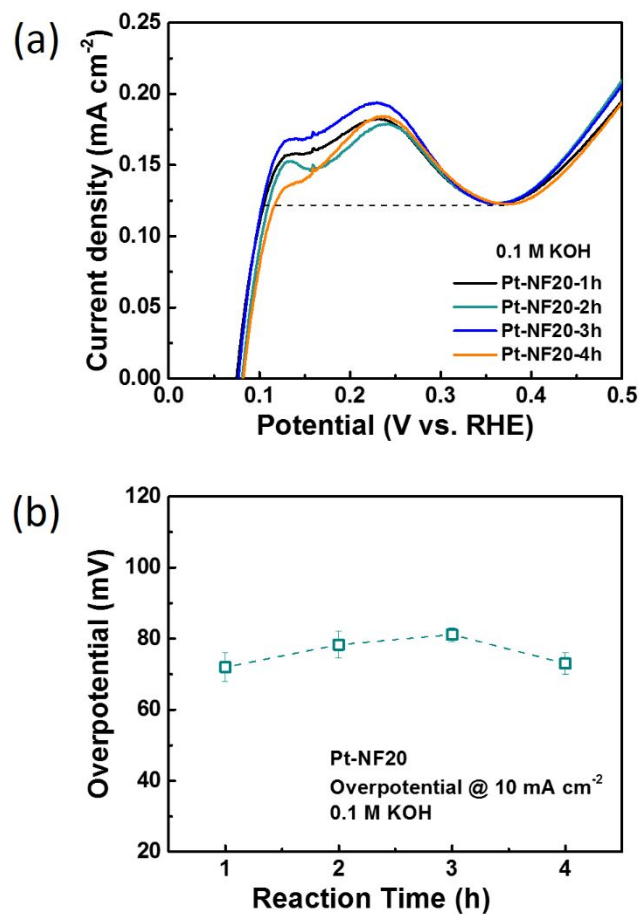


Figure S18. The optimization of deposition time for Pt-NF20 under 40 °C from 1 h to 4 h. (a) ECSA of Pt and (b) HER overpotential at 10 mA cm<sup>-2</sup> via galvanostatic method for 180 s tested in 0.1 M KOH. To diminish the effect of Ni(OH)<sub>2</sub> producing during deposition Pt, the deposition time was chosen of 1 h.

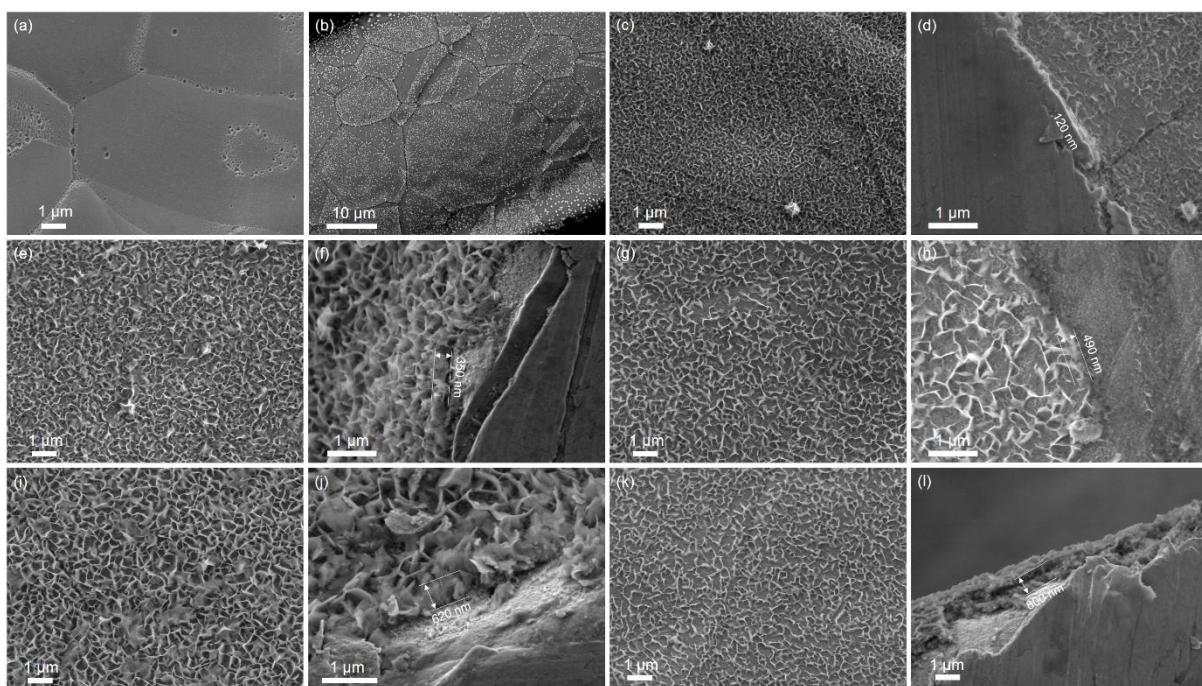


Figure S19. SEM images of (a) Pt-NF20, (b) Pt-NF20 under mode of BED, (c, d) Ni(OH)<sub>2</sub>-2h-Pt-NF20, (e, f) Ni(OH)<sub>2</sub>-4h-Pt-NF20, (g, h) Ni(OH)<sub>2</sub>-6h-Pt-NF20, (i, j) Ni(OH)<sub>2</sub>-8h-Pt-NF20 and (k, l) Ni(OH)<sub>2</sub>-10h-Pt-NF20 electrodes.

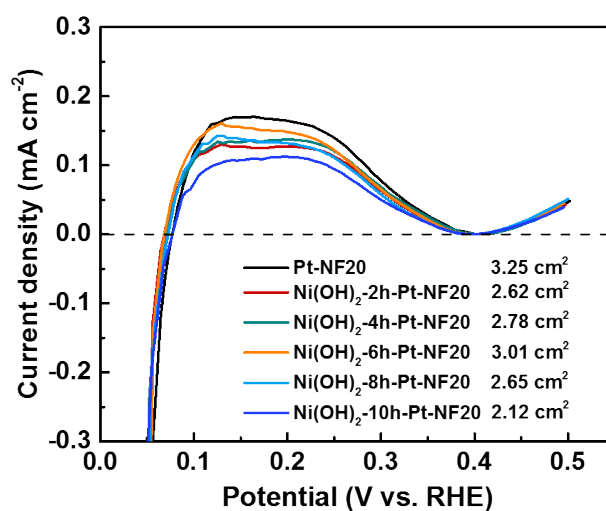


Figure S20. The partial CV curves with background correction of Pt-NF20, Ni(OH)<sub>2</sub>-2h-Pt-NF20, Ni(OH)<sub>2</sub>-4h-Pt-NF20, Ni(OH)<sub>2</sub>-6h-Pt-NF20, Ni(OH)<sub>2</sub>-8h-Pt-NF20 and Ni(OH)<sub>2</sub>-10h-Pt-NF20

electrodes for ECSA of Pt in 0.1 M KOH at a scan rate of 50 mV s<sup>-1</sup>.

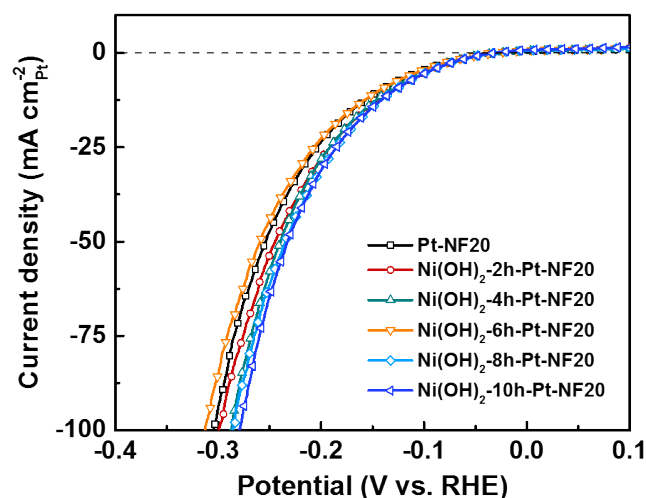


Figure S21. The HER polarization curves normalized to ECSA of Pt for the Pt-NF20, Ni(OH)<sub>2</sub>-2h-Pt-NF20, Ni(OH)<sub>2</sub>-4h-Pt-NF20, Ni(OH)<sub>2</sub>-6h-Pt-NF20, Ni(OH)<sub>2</sub>-8h-Pt-NF20 and Ni(OH)<sub>2</sub>-10h-Pt-NF20 electrodes.

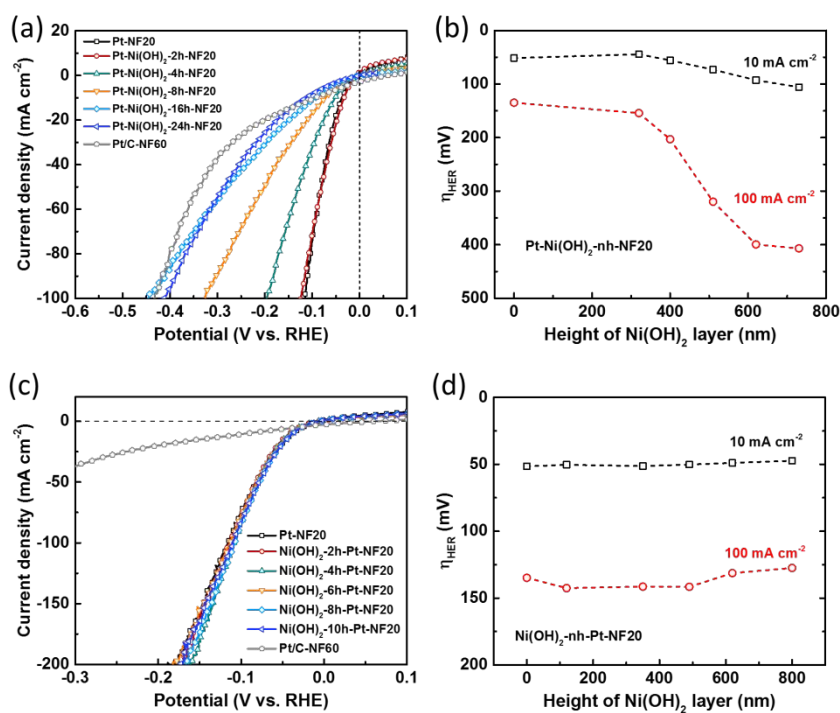


Figure S22. HER performance in 0.5 M PB. (a) HER polarization curves of the Pt-NF20, Pt-Ni(OH)<sub>2</sub>-nh-NF20 and Pt/C-NF60 electrodes. (b) HER overpotentials with different height of Ni(OH)<sub>2</sub> layers

at the current density of 10 and 100 mA cm<sup>-2</sup> via galvanostatic method as taking records at 180 s. (c) HER polarization curves of the Pt-NF20, Ni(OH)<sub>2</sub>-nh-Pt-NF20 and Pt/C-NF60 electrodes. (d) HER overpotentials with different height of Ni(OH)<sub>2</sub> layers at the current density of 10 and 100 mA cm<sup>-2</sup> via galvanostatic method as taking records at 180 s.

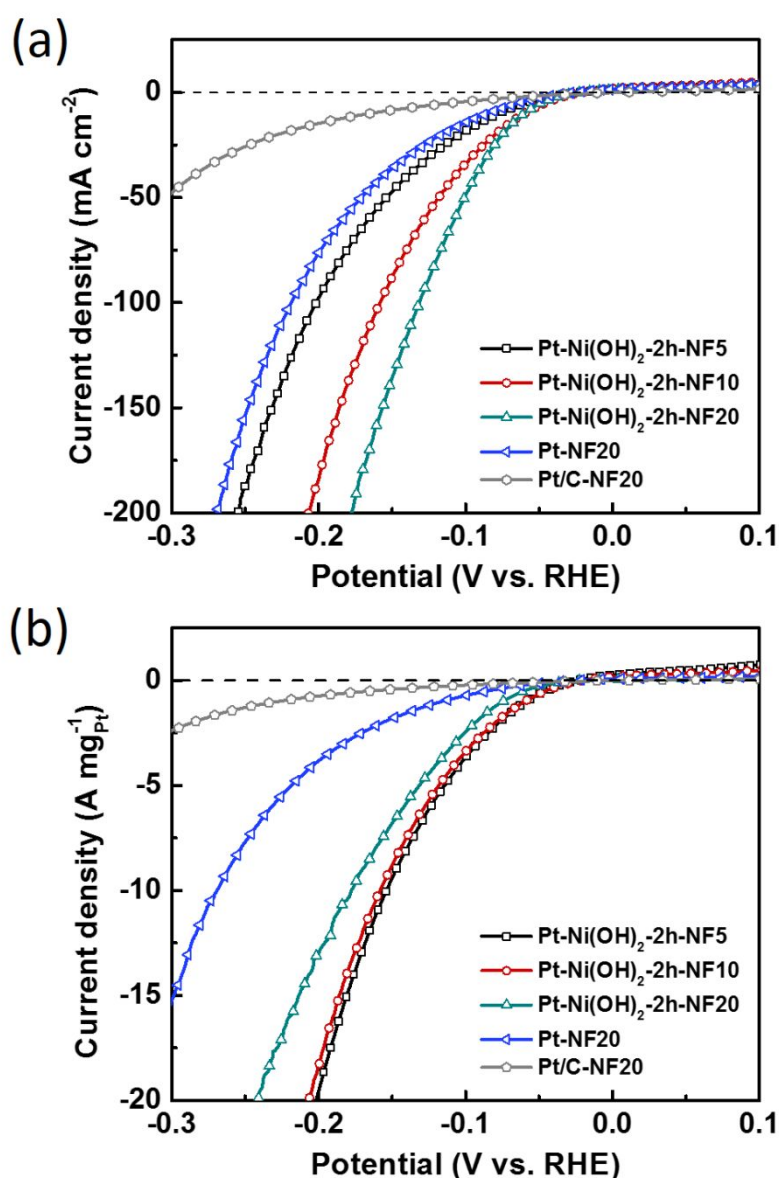


Figure S23. HER LSV curves of (a) normalizing to geometric area and (b) mass of Pt for Pt-Ni(OH)<sub>2</sub>-2h-NF5, Pt-Ni(OH)<sub>2</sub>-2h-NF10, Pt-Ni(OH)<sub>2</sub>-2h-NF20, Pt-NF20 and Pt/C-NF20 electrodes.

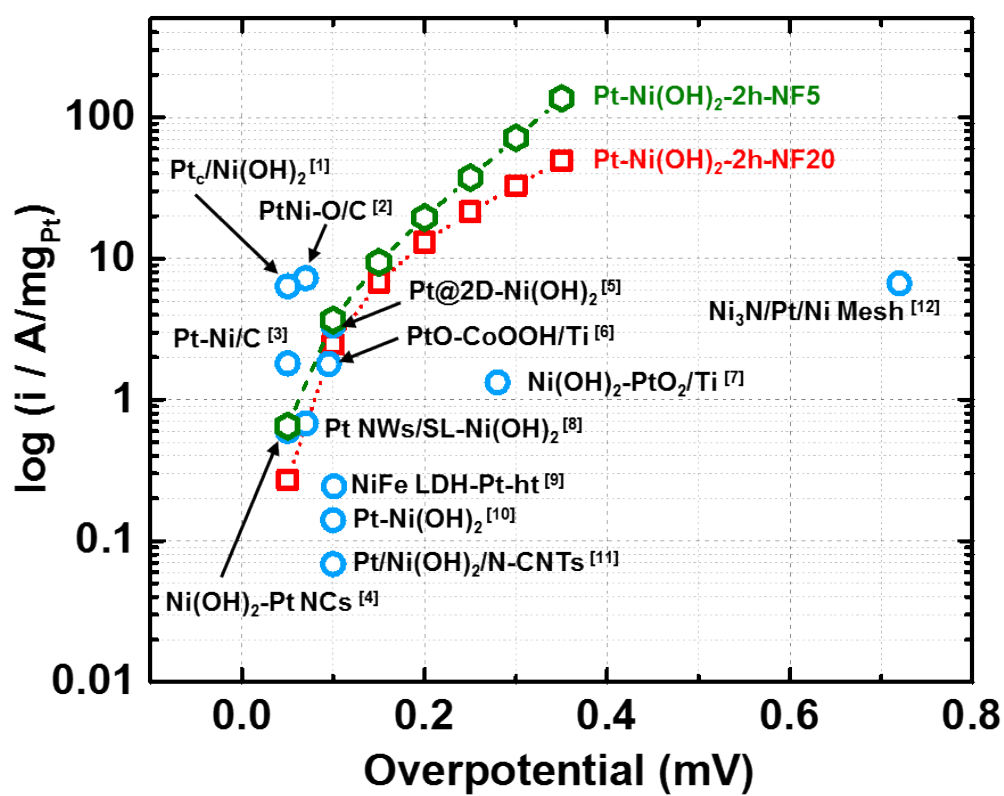


Figure S24. HER performance comparison of Pt-Ni(OH)<sub>2</sub>-2h-NF5 and Pt-Ni(OH)<sub>2</sub>-2h-NF20 electrodes with the state of art literatures. Current densities were normalized to the specific mass of Pt.

## References

- (1) Hong, Y.; Choi, C. H.; Choi, S. I. Catalytic Surface Specificity of Ni(OH)<sub>2</sub>-Decorated Pt Nanocubes for the Hydrogen Evolution Reaction in an Alkaline Electrolyte. *ChemSusChem* 2019, 12, 4021-4028.
- (2) Zhao, Z.; Liu, H.; Gao, W.; Xue, W.; Liu, Z.; Huang, J.; Pan, X.; Huang, Y. Surface-Engineered PtNi-O Nanostructure with Record-High Performance for Electrocatalytic Hydrogen Evolution Reaction. *J. Am. Chem. Soc.* **2018**, 140, 9046-9050.
- (3) Kaviani, R.; Choi, S.I.; Park, J.; Liu, T.; Peng, H.-C.; Lu, N.; Wang, J.; Kim, M. J.; Xia, Y.; Lee, S. W. Pt-Ni Octahedral Nanocrystals as a Class of Highly Active Electrocatalysts toward the Hydrogen Evolution Reaction in an Alkaline Electrolyte. *J. Mater. Chem. A* **2016**, 4, 12392-12397.
- (4) Yang, H. C.; Wang, C. H.; Hu, F.; Zhang, Y. J.; Lu, H.; Wang, Q. B. Atomic-Scale Pt Clusters Decorated on Porous Alpha-Ni(OH)<sub>2</sub> Nanowires as Highly Efficient Electrocatalyst for Hydrogen Evolution Reaction. *Sci. China, Mater.* **2017**, 60, 1121-1128.
- (5) Wang, L.; Zhu, Y. H.; Zeng, Z. H.; Lin, C.; Giroux, M.; Jiang, L.; Han, Y.; Greeley, J.; Wang, C.; Jin, J. Platinum-Nickel Hydroxide Nanocomposites for Electrocatalytic Reduction of Water. *Nano Energy* **2017**, 31, 456-461.
- (6) Wang, Z.; Ren, X.; Shi, X.; Asiri, Abdullah M.; Wang, L.; Li, X.; Sun, X.; Zhang, Q.; Wang, H. A Platinum Oxide Decorated Amorphous Cobalt Oxide Hydroxide Nanosheet Array towards Alkaline Hydrogen Evolution. *J. Mater. Chem. A* **2018**, 6, 3864-3868.
- (7) Xie, L.; Ren, X.; Liu, Q.; Cui, G.; Ge, R.; Asiri, A. M.; Sun, X.; Zhang, Q.; Chen, L. A Ni(OH)<sub>2</sub>-PtO<sub>2</sub> Hybrid Nanosheet Array with Ultralow Pt Loading toward Efficient and Durable Alkaline Hydrogen Evolution. *J. Mater. Chem. A* **2018**, 6, 1967-1970.

- (8) Yin, H.; Zhao, S.; Zhao, K.; Muqsit, A.; Tang, H.; Chang, L.; Zhao, H.; Gao, Y.; Tang, Z. Ultrathin Platinum Nanowires Grown on Single-Layered Nickel Hydroxide with High Hydrogen Evolution Activity. *Nat. Commun.* **2015**, *6*, 6430.
- (9) Anantharaj, S.; Karthick, K.; Venkatesh, M.; Simha, T.; Salunke, A. S.; Ma, L.; Liang, H.; Kundu, S. Enhancing Electrocatalytic total Water Splitting at Few Layer Pt-NiFe Layered Double Hydroxide Interfaces. *Nano Energy* **2017**, *39*, 30-43.
- (10) Jung, E.; Park, H. Y.; Cho, A.; Jang, J. H.; Park, H. S.; Yu, T. Aqueous-Phase Synthesis of Metal Hydroxide Nanoplates and Platinum/Nickel Hydroxide Hybrid Nanostructures and Their Enhanced Electrocatalytic Properties. *Appl. Catal. B Environ.* **2018**, *225*, 238-242.
- (11) Wang, Y.; Qin, Y.; Zhang, X.; Dai, X.; Zhuo, H.; Luan, C.; Jiang, Y.; Zhao, H.; Wang, H.; Huang, X. Promoting Effect of Nickel Hydroxide on the Electrocatalytic Performance of Pt in Alkaline Solution. *Dalton Trans.* **2018**.
- (12) Wang, Y.; Chen, L.; Yu, X.; Wang, Y.; Zheng, G. Superb Alkaline Hydrogen Evolution and Simultaneous Electricity Generation by Pt-Decorated Ni<sub>3</sub>N Nanosheets. *Adv. Energy Mater.* **2017**, *7*, 1601390.